



**HAL**  
open science

# Clay/phosphate-based ceramic materials for thermal energy storage – Part I: Effect of synthetic phosphate content on microstructure, thermo-physical and thermo-mechanical properties

Abdoul Razac Sane, Doan Pham Minh, Nawal Semlal, Rachid Boulif, Claudia Toussaint, Alain Germeau, Ange Nzihou

## ► To cite this version:

Abdoul Razac Sane, Doan Pham Minh, Nawal Semlal, Rachid Boulif, Claudia Toussaint, et al.. Clay/phosphate-based ceramic materials for thermal energy storage – Part I: Effect of synthetic phosphate content on microstructure, thermo-physical and thermo-mechanical properties. *Open Ceramics*, 2023, 14, pp.100346. 10.1016/j.oceram.2023.100346 . hal-04050915

HAL Id: hal-04050915

<https://imt-mines-albi.hal.science/hal-04050915v1>

Submitted on 3 Apr 2023

**HAL** is a multi-disciplinary open access archive for the deposit and dissemination of scientific research documents, whether they are published or not. The documents may come from teaching and research institutions in France or abroad, or from public or private research centers.

L'archive ouverte pluridisciplinaire **HAL**, est destinée au dépôt et à la diffusion de documents scientifiques de niveau recherche, publiés ou non, émanant des établissements d'enseignement et de recherche français ou étrangers, des laboratoires publics ou privés.



Distributed under a Creative Commons Attribution - NonCommercial - NoDerivatives 4.0 International License



# Clay/phosphate-based ceramic materials for thermal energy storage – Part I: Effect of synthetic phosphate content on microstructure, thermo-physical and thermo-mechanical properties

Abdoul Razac Sane<sup>a,\*,\*\*</sup>, Doan Pham Minh<sup>a,\*</sup>, Nawal Semlal<sup>b</sup>, Rachid Boulif<sup>b</sup>,  
Claudia Toussaint<sup>c</sup>, Alain Germeau<sup>c</sup>, Ange Nzihou<sup>a</sup>

<sup>a</sup> Université de Toulouse, IMT Mines Albi, CNRS UMR 5302, Centre RAPSODEE, Campus Jarlard, F-81013, Albi Cedex 09, France

<sup>b</sup> Innovation, OCP SA, BP 118, 24000, El Jadida, Morocco

<sup>c</sup> PRAYON S.A., Rue J. Wauters, 144, B-4480, Engis, Belgium

## ARTICLE INFO

Handling Editor: Dr P Colombo

### Keywords:

Phosphate

Clay

Microstructure

## ABSTRACT

Fired clay ceramics are promising materials for TES, thanks to their thermal stability, availability worldwide, low cost and easy shaping and handling. However, their thermo-physical and thermo-mechanical properties have to be improved. For the first time, clay-phosphate ceramics, with synthetic calcium hydroxyapatite (TCP,  $\text{Ca}_{10}(\text{PO}_4)_6(\text{OH})_2$ ) as additive, were developed in view of TES application. A parametric study was carried out for different clay/TCP mixtures, wherein the TCP percentage varies from 0 to 16.7 wt%. The best material containing 4.7 wt% TCP allowed increasing up to 20% of the thermal conductivity and 23% of the mechanical strength. Moreover, it was thermally stable up to 1000 °C. These original results demonstrate the suitability of these new materials for heat storage in energy systems such as in a concentrated solar power (CSP) plant, or in a unit of heat recovery from an industrial waste heat source.

## 1. Introduction

One of the most important challenges that our society faces is the satisfactory supply, dispatchability and management of the energy. In this context, a successful and efficient exploitation of all energetic resources, fossil and renewable, will be the key factor in order to reach a fair and equitable distribution of the available energy. Even if fossil energies currently remain the main energetic resource, which make up *ca.* 80% of the world energy production, they are expected to be reduced in the next decades in favor of alternative renewable energies [1,2].

Among different types of renewable energy, solar energy appears as the most abundant source and can be accessible from different countries. Solar photovoltaic (PV) and concentrated solar power (CSP) are the two main technologies developed for solar energy [1,3,4]. CSP presents several strategic advantages, principally the possibility of heat storage integration, which allows improving the efficiency of the plant and limiting the intermittent character of the solar source as well as its seasonal effect [5–8]. Typically, it allows adapting the production to the demand and equilibrating the energy generation avoiding undesirable

production peak. This makes thermal energy storage (TES) systems as an integral part of CSP plants and contributes of energy cost reduction [6,8,9]. There are three concepts for heat storage: sensible, latent and thermochemical heat storage [10–12]. In all cases, a storage media is needed. Currently, only sensible storage is used in industrial CSP plants with molten salts as storage media used in the liquid form in two tanks technologies [6,13,14]. Typical example of CSP plants in operation with this technology is Andasol located in Spain using more than 28,500 tons of molten salts and generates approximately 200 GWh per year [15–17]. It is also the case of NOOR I in Morocco inaugurated in 2016 with 160 MW capacity which integrates a storage capacity of 3 h (molten salt as TES media) [18]. In 2014, IEA has predicted that CSP will contribute to 11% of the world electricity production by 2050 [19]. This requires a nitrate salt consumption around 20–30 times higher than the current worldwide production from nitrate mines [19]. In addition, the use of nitrate salts as TES media has several disadvantages related to the high cost due to the quality required, corrosion, low thermal conductivity (0.55 W/m/K at 400 °C) and stability, competition with other sectors (for examples: agriculture and chemical industries), and low operational

\* Corresponding author.

\*\* Corresponding author.

E-mail addresses: [asane@mines-albi.fr](mailto:asane@mines-albi.fr) (A.R. Sane), [doan.phamminh@mines-albi.fr](mailto:doan.phamminh@mines-albi.fr) (D. Pham Minh).

**Table 1**  
Main parameter of X-ray tomography analysis.

X-ray source	ESRF - European Synchrotron Radiation Facility, ID19 (Grenoble, France)
Energy level	35 keV
Projection number	3500
Exposure time	0.06 s
Analysis volume	1.6 × 1.6 × 1.3 mm <sup>3</sup>

**Table 2**  
Elemental composition of clay and TCP used in this work.

Samples	Concentration (wt.%)							
	SiO <sub>2</sub>	Al <sub>2</sub> O <sub>3</sub>	CaO	Fe <sub>2</sub> O <sub>3</sub>	K <sub>2</sub> O	MgO	Na <sub>2</sub> O	P <sub>2</sub> O <sub>5</sub>
Clay	45.8	16.2	8	8.5	4.3	1.3	0.2	–
TCP	–	–	55.8	–	–	–	–	42.4

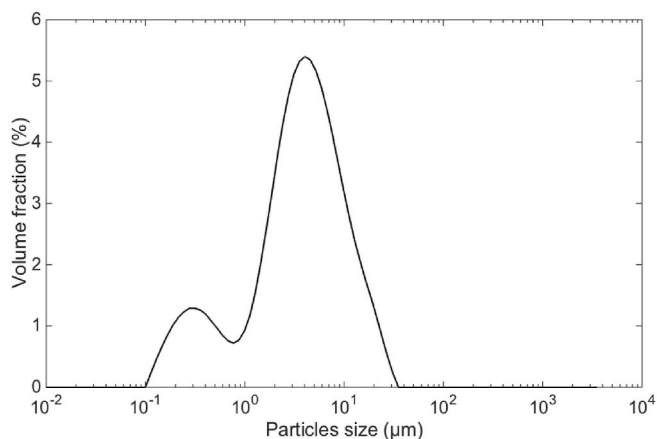


Fig. 1. Particle size distribution of the TCP used in this work.

temperature range limited between 225 and 600 °C [14,20]. So, molten salts are not adapted to high temperature applications, such as solar power tower technology, where temperatures can reach 1000 °C [6,21]. Hence, there is currently an urgency to develop new performing TES materials in order to support next generation of CSP plants.

In this context, research efforts are devoted to the development of alternative materials that could be used as storage media in a new

generation system called thermocline; a breakthrough concept that can be used to store heat from CSP plants as well as industrial heat recovery. The development of alternative TES materials is based on the control of different criteria including the availability at the industrial scale, low cost, easy processing, acceptable eco-balance, high thermo-mechanical stability and compatibility with the heat transfer fluid (HTF) [22,23]. A wide range of attractive materials has been identified and studied for TES applications and can be grouped as natural rocks, concrete and

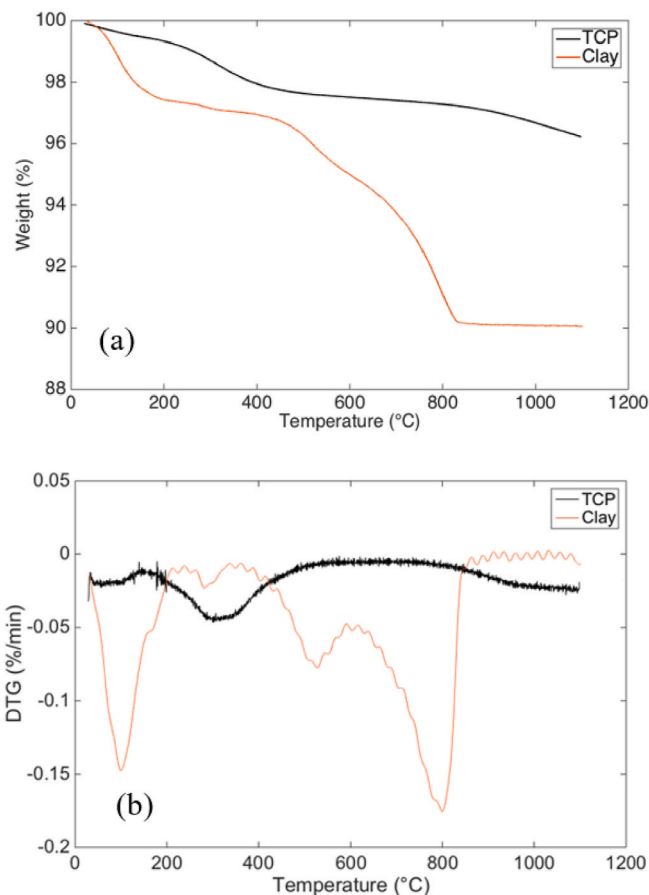


Fig. 3. TG (a) and DTG (b) curves of the raw materials under air atmosphere (heating rate of 5 °C/min).

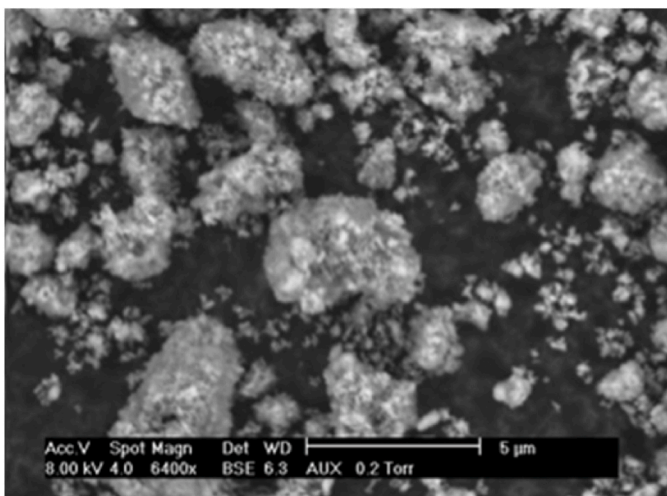
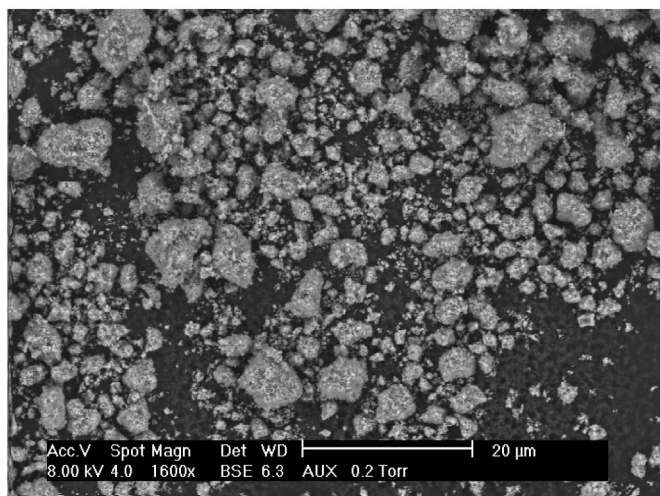


Fig. 2. Illustration of SEM images of TCP powder used in this work.

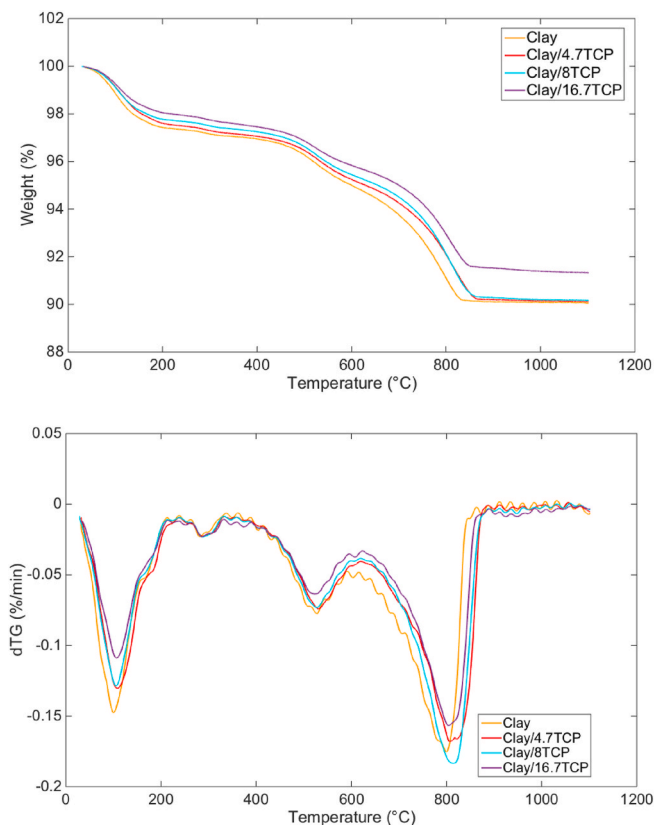


Fig. 4. TG and dTG curves of the clay ceramic and clay ceramics doped with 4.7, 8 and 16.7 wt % of TCP.

ceramics.

A large number of research works have investigated the thermo-physical and thermo-mechanical properties of various rock types [24–27]. However, most of them are generally not suitable for high temperature storage (>600 °C). For example, results obtained by

Tiskatine et al. who investigated the thermal cycling resistance of various rocks have shown that many types of rocks are unsuitable for high temperature use because of deterioration of properties due to the formation of microcracks. In addition, mineralogical composition, geological age, impurities and heterogeneity of natural rocks can affect their use in large industrial scale because they lead to the variation of physical, thermal and mechanical properties [28]. This limits the use of natural rocks as TES materials.

Concrete is easy to process, is largely available, and has interesting thermo-physical properties. Several research works have been devoted to the investigation of concrete as TES materials at pilot scale [9,29–31]. The common findings of these works showed that concrete is suitable for sensible heat storage, but it is not adapted for high temperature applications. In fact, results obtained by Laing et al. [29] shown that the compressive strength of concrete decreased from 29 to about 15 N/mm<sup>2</sup> after several thermal cycles at a temperature of 500 °C. This was also observed by John et al. [32]. This means that the use of concrete is limited only for low temperature storage technologies (e.g. below 400 °C). In contrast, ceramic materials are generally suitable for high temperature applications. On the one hand, a great number of research studies are focused on the development of ceramics from the valorization of industrial waste and by-products (asbestos-containing wastes, fly ash, slag from electric arc furnace steelmaking processes) into TES materials [22,33–35]. The most challenging aspect in this area is the complexity in the raw materials shaping. In fact, high temperature processes, such as plasma processing, have been investigated for the processing of those materials. However, it came to an issue due to the high energetic and economical cost. On the other hand, clay based ceramics were longtime used as bricks and tiles for building applications [36]. They have potential to be used as TES materials thanks to their thermal stability up to 1000 °C, availability worldwide in large quantity, easy shaping and handling using a basic production process by extrusion, and low cost [37,38]. However, the thermo-physical and thermo-mechanical properties of traditional clay ceramics have to be improved to meet criteria of TES materials.

Hence, the objective of this work is to investigate the microstructure, the thermo-physical and thermo-mechanical properties of the clay ceramics doped with phosphate (TCP) to develop an alternative TES material. TCP was chosen as additive because it has the criteria required for

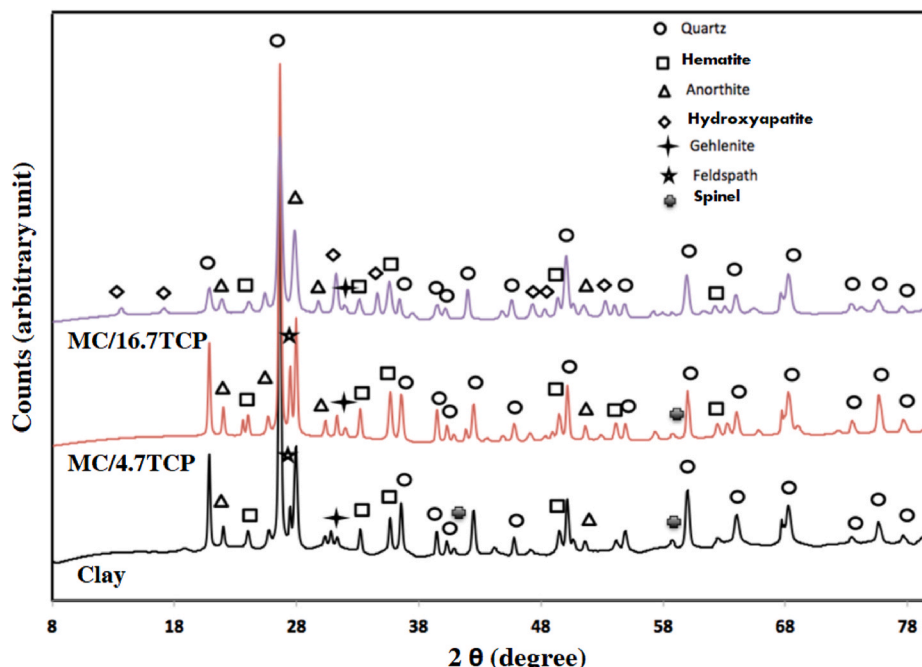
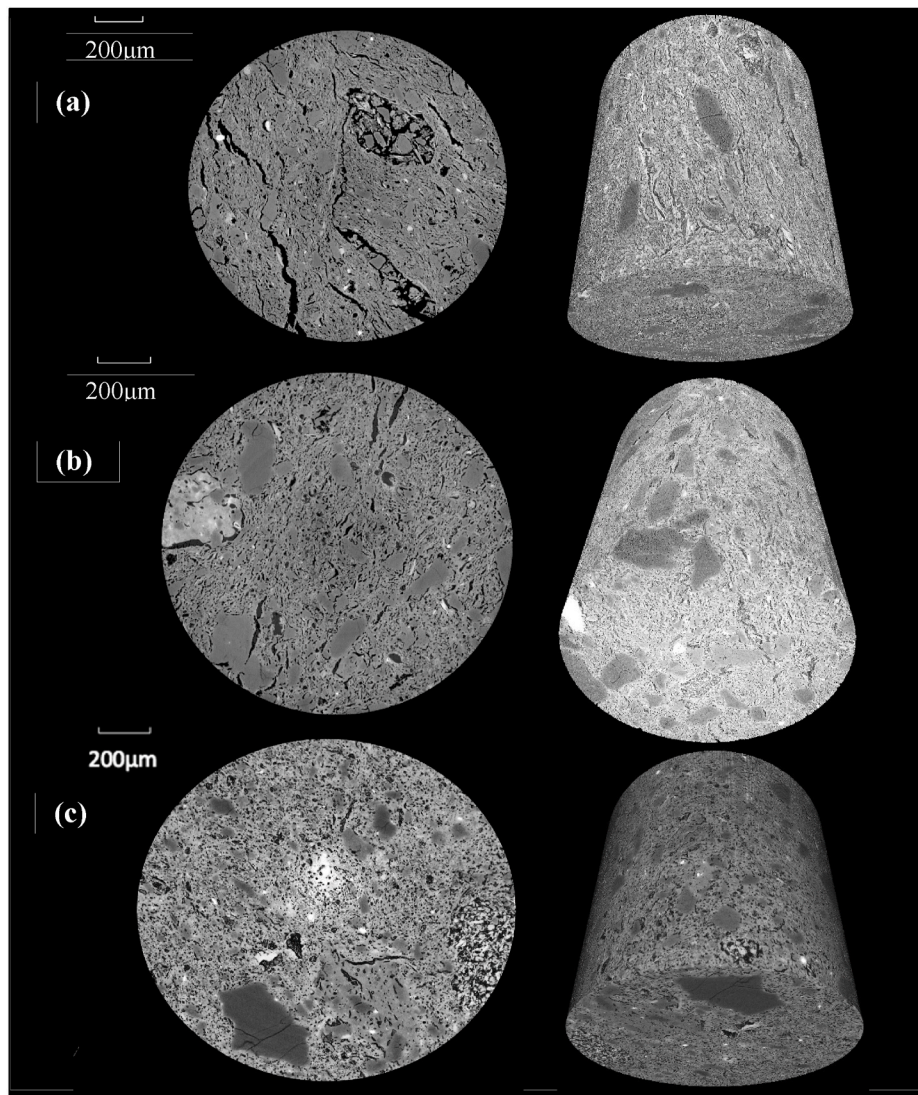


Fig. 5. XRD patterns of the ceramics after firing at 1100 °C.



**Fig. 6.** X-ray tomography micrographs of the fired ceramics: cross-section and 3D representations. (a): Virgin clay ceramic without TCP; (b): Clay/4.7TCP; (c): Clay/16.7TCP. Firing conditions: 5 °C/min heating rate, 1100 °C final temperature, under air atmosphere.

a TES material, in particular its high thermal stability at high temperature (>1000 °C) without significant decomposition, and interesting thermo physical properties [39,40]. To the best of our knowledge, the present study is the first work dedicated to the development of clay-phosphate ceramic materials for TES application.

## 2. Materials and experimental methods

### 2.1. Raw materials

The clay used in this study is a mixture of clay minerals and sand (80/20 wt%) extracted from a quarry in southwest of France, which was provided by a brickyard in the Occitanie region. Commercial hydroxyapatite (3 g/cm<sup>3</sup> true density, under the fine powder form), named TCP in this work, provided by PRAYON S.A (Belgium) was used as additive without further modification. The main characteristics of the raw materials are presented in the results section.

### 2.2. Production of the clay ceramics

The clay ceramics investigated in this work were obtained by mixing clay, TCP and water. Their production was carried out with equipment

provided by our industrial partner, who is a world leader in brick and tile production. For a given preparation, the mixture of clay and TCP (2, 4.7, 8, 12 or 16.7 wt%) was prepared in a kneading bowl for 5–7 min, with a gradual addition of water up to 15 wt%. The corresponding products are named as *Clay/xTCP*, with *x* represents TCP content (wt. %). The mixture was then extruded using a bench extruder (Bongioanni) at 7.5–8 bar pressure to form ceramic blocks of 170 × 75 × 13 mm<sup>3</sup>. Those blocks were progressively dried at 25, 45, 65 and 105 °C, with a plateau time of 24 h at each temperature, in an electrical oven (Memmert). From these dried ceramic blocks, samples for different characterizations were prepared using an electric circular saw to get desired shape and size, and polished with P80, P120, P180 or P280 SiC abrasive paper (CarbiMet). Finally, fired ceramics were obtained by calcination at 1100 °C (5 °C/min heating rate) in an electrical furnace (Controller P320, Nabertherm).

### 2.3. Analyses and characterizations

Different analysis and characterizations were performed with both raw materials and fired ceramics.

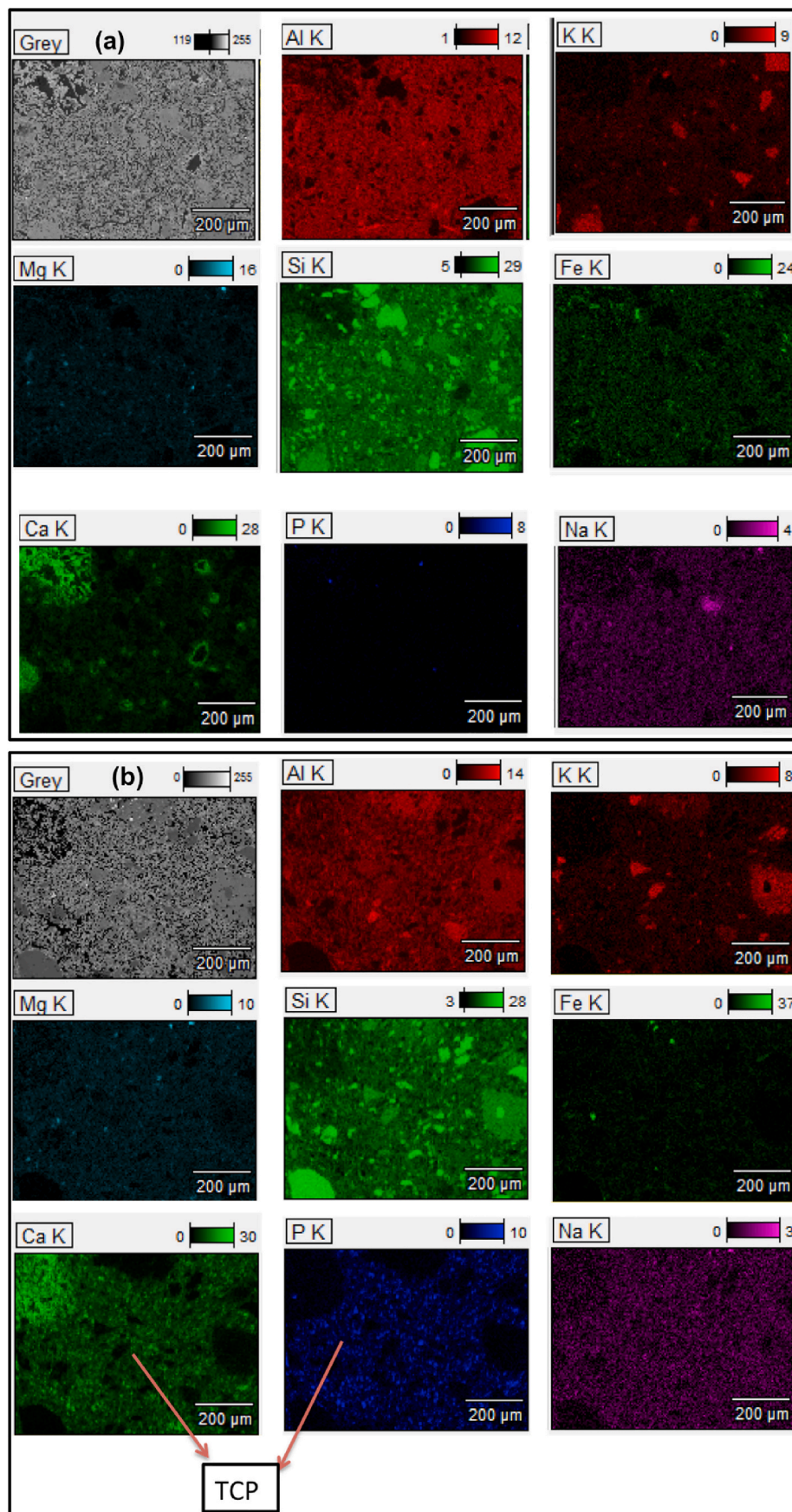


Fig. 7. Imaging of the main elements present in: (a) virgin clay ceramic without TCP addition; (b) and Clay/16.7TCP, after firing at 1100 °C (5 °C/in heating) under air atmosphere.

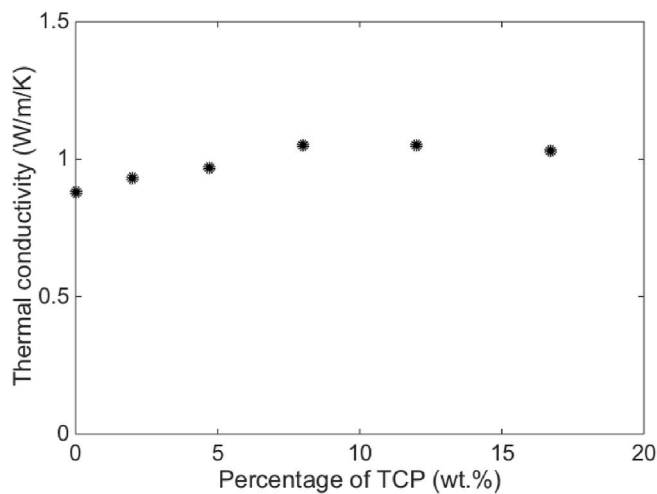


Fig. 8. Evolution of thermal conductivity of fired ceramics as a function of TCP content. Firing conditions: 5 °C/min heating rate, 1100 °C final temperature, under air atmosphere.

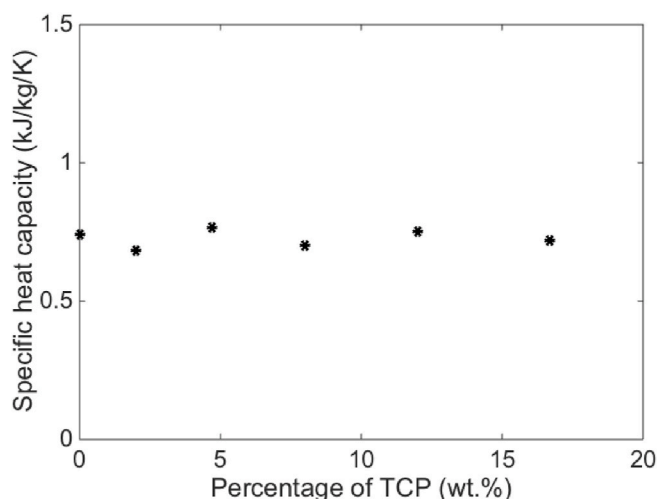


Fig. 9. Evolution of specific heat capacity of fired ceramics as a function of TCP content. Firing conditions: 5 °C/min heating rate, 1100 °C final temperature, under air atmosphere.

### 2.3.1. Elemental composition, particle size distribution and thermal behavior

The elemental composition of the clay was obtained with an ICP-AES instrument (Jobin Yvon Ultima 2). Before the analysis, the clay was firstly dissolved in a mixture of fluoric, nitric and sulfuric acid at 200 °C during one night in a Teflon-coated sealed autoclave. The solution was diluted 10 times in permuted water. The measurement was repeated at least twice for each sample.

The particle size distribution of TCP was measured using laser granulometry analysis (Mastersizer 3000, Malvern). The measurements were performed in the dry medium (air).

The thermal behavior of ceramics was carried out via thermogravimetry analysis (TG) using an Q600 apparatus (TA Instruments), in the temperature range of 30–1100 °C (5 °C/min heating rate) under an air flow (3 NL/h). For each measurement, a cylinder of ca. 200 mg of fired ceramic was used.

### 2.3.2. Density, pore volume fraction and microstructure observations

Pore volume fraction and bulk density were measured using a water adsorption technique [41]. The measurements were performed with

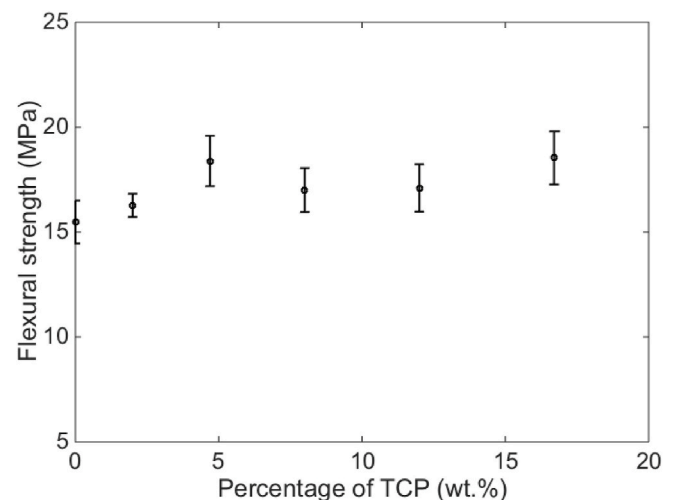


Fig. 10. Evolution of flexural strength of fired ceramics as a function of TCP content. Firing conditions: 5 °C/min heating rate, 1100 °C final temperature, under air atmosphere.

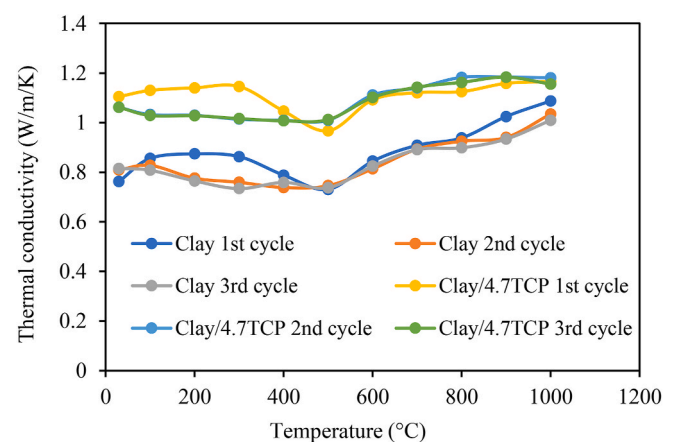


Fig. 11. Thermal conductivity of the fired ceramics during three consecutive heating cycles. Conditions: 5 °C/min heating rate, air atmosphere.

samples of 30 × 30 × 5 mm<sup>3</sup>. Firstly, the samples were introduced in a vacuum chamber and maintained under a residual pressure of 30 kPa for 4 h. Some water was then introduced in the vacuum chamber up to partial immersion of the samples. The samples remained partially immersed under the same residual pressure of 30 kPa for 2 h. Subsequently, the samples were subjected to full immersion in the water. The full immersion of the samples was maintained for 24 h. The atmospheric pressure was finally restored in the vacuum chamber. The samples remained immersed at atmospheric pressure for 24 more hours. Following this operation, the weight of the samples was measured under three different conditions. It was measured under air, under water by hydrostatic weighing and under air after wet wiping. The bulk density ( $\rho_{\text{Bulk}}$ ) and the percentage of porosity ( $\epsilon$ ) of the samples could be respectively calculated from Eq. (1) and Eq. (2) [41], where  $W_h$  is the hydrostatic weight,  $W_w$  is the wet weight, and  $W_d$  is the dry weight. The measurement was repeated at least twice for each sample. These measurements were performed at room temperature (ca. 20 °C).

$$\rho_{\text{Bulk}} = \frac{W_d}{W_w - W_h} \quad \text{Eq. 1}$$

$$\epsilon = \frac{W_w - W_d}{W_w - W_h} \times 100\% \quad \text{Eq. 2}$$

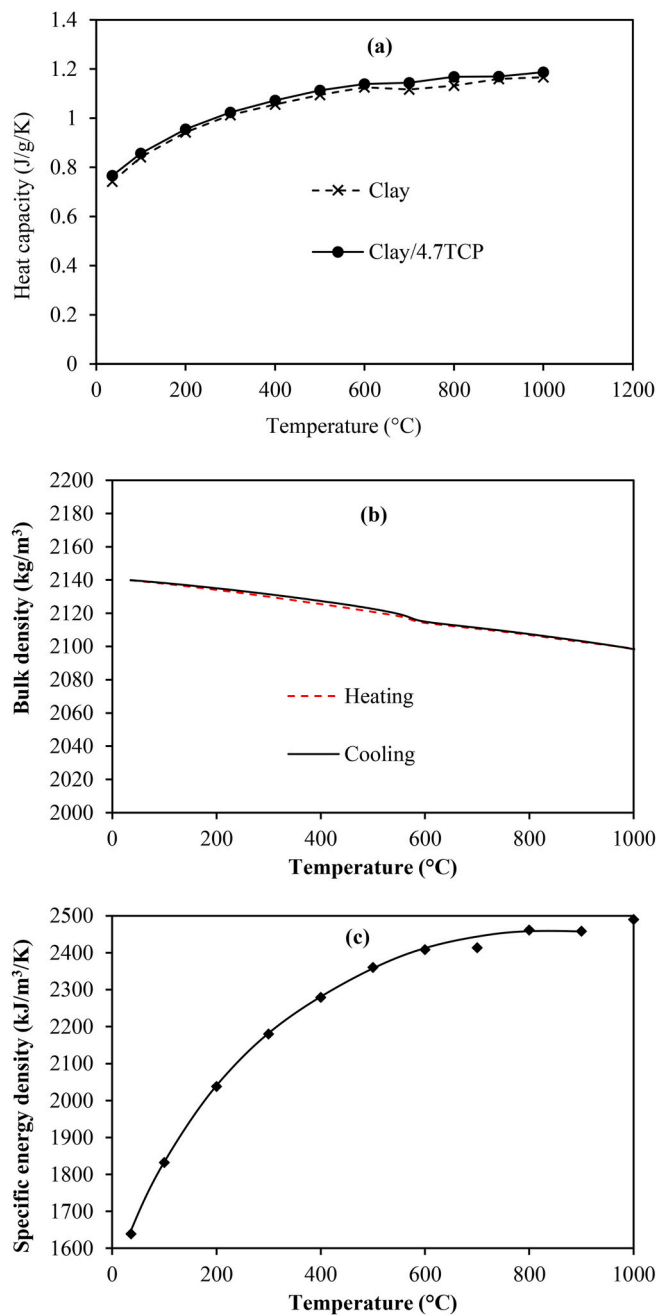


Fig. 12. (a) Specific heat capacity, (b) bulk density (determined from TMA and TG analyses), and (c) specific energy density of the fired ceramic as functions of the temperature.

X-ray diffraction (XRD) measurements were carried out with a Philips Panalytical Pro MPD. The identification of crystalline phases was performed by comparison of the measured patterns with JCPDS (Joint Committee on Powder Diffraction Standards) database.

The microstructure of the clay-based ceramics was observed by X-ray tomography using the Synchrotron facility. The samples were firstly fired at 1100 °C. Then, cylinders of *ca.* 150 mg were prepared by polishing technique, without using resin to embed the samples. Table 1 shows the main analysis parameters used. To build 3D structure, a series of radiographs were acquired under different angles of measurement by rotating the sample. Then, the cross-sections scans were used to build 3D representations of the samples where the solid skeleton was presented in light grey color and the porosity in a black color.

Scanning electron microscopy coupled with energy dispersive

spectroscopy (SEM-EDX) was carried out with a machine of FEI Company (Philips XL30 ESEM). This technique mostly allows imaging chemical elements present on the surface of a sample at the micrometric scale.

### 2.3.3. Measurement of the thermal conductivity and specific heat capacity

The thermal properties of the fired ceramics were determined at room temperature (static measurement) or at higher temperatures (dynamic measurement).

At room temperature, the thermal conductivity ( $\lambda$ ) measurements were performed with  $30 \times 30 \times 5 \text{ mm}^3$  samples using the transitory plane source method (TPS 2500, Hot Disk AB). The data were treated with algorithms of the Thermal Constant Analyzer. The modulated DSC (MDSC Q200, TA Instrument) was used for the measurement of specific heat capacity ( $C_p$ ). Those measurements were repeated at least twice for each sample.

Dynamic measurements were performed using the Laser Flash method in a NETZSCH laser flash apparatus (Microflash LFA 457). The measurements were performed with fired samples of  $10 \times 10 \times 1.5 \text{ mm}^3$  under the air atmosphere from 30 to 1000 °C (5 °C/min heating rate). Details of the measurement will be presented in Section 3.5. The thermal diffusivity ( $\varphi$ ) is recorded as a function of the temperature. The thermal conductivity ( $\lambda$ ) is deduced from Eq. (3) [42]:

$$\lambda(T) = \rho(T) \times C_p(T) \times \varphi(T) \quad \text{Eq. 3}$$

where  $\rho$  is the bulk density,  $C_p$  is the specific heat capacity and  $\varphi$  is the thermal diffusivity.  $\rho(T)$  was obtained in a SETSYS Evolution apparatus (TMA 1600, SETARAM), while  $C_p(T)$  was obtained with a DSC 404 F1 Pegasus (NETZSCH). The measurements of  $C_p(T)$  were performed under Ar flux (50 NmL/min) within the temperature range of 30–1000 °C (20 °C/min heating rate). Cylindrical samples of 4 mm diameter and 1.3 mm length were employed.

### 2.3.4. Measurement of the mechanical and thermomechanical properties

The mechanical properties of the fired ceramics were determined at room temperature (static measurement) or at higher temperatures (dynamic measurement).

At room temperature, the measurements were carried out in an Instron 5800 R, using a three-point bend testing fixture (load span of 40 mm) and a 500 N load cell. The specimens with dimensions of  $60 \times 10 \times 5 \text{ mm}^3$  were subjected to a constant displacement rate of 1 mm/min until the fracture. The measurement was repeated at least three times for each sample to get the average value. The flexural strength of the fired clay ceramics ( $\sigma_f$ ) was calculated from Eq. (4) [43], where  $F_{\text{Max}}$  is the maximum force (which is obtained with Instron 5800 R apparatus),  $L$  is the loading span,  $B$  is the breadth, and  $H$  is the height of the flexural samples.

$$\sigma_f = \frac{3 \times F_{\text{Max}} \times L}{2 \times B \times H^2} \quad \text{Eq. 4}$$

For the dynamic measurement, the Young's modulus was continuously measured from room temperature to 1050 °C by a resonant frequency analyzer (IMCE HT650), equipped with a flexural mode. Details of the measurement will be presented in Section 3.5. The Young's modulus was calculated from the resonance frequency, and the sample dimension and weight, according to the norm ASTM E1876 [44].

Thermomechanical analysis (TMA) was determined with a SETARAM SETSYS Evolution TMA 1600 apparatus. For each measurement, ceramic sample was fired at 1050 °C under the air atmosphere. Then, it was polished to reach the initial cylindrical dimension of 0.6 cm diameter and 1.4 cm length. The analysis was done from 30 to 1000 °C (5 °C/min heating rate) under the air flux (3 NL/h) and under a constant charge of 10 g. The variation of the dimension was monitored along the analysis at each interval of 5 °C. From the variation of dimension by TMA, the variation of mass by TG under similar conditions, and the

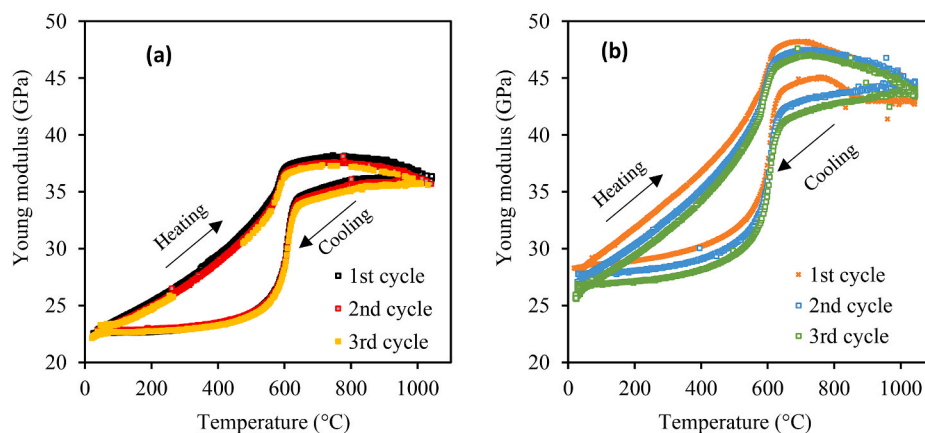


**Fig. 13.** Young's modulus of: (a) fired virgin clay ceramic, (b) and fired Clay/4.7TCP ceramic during three consecutive heating/cooling cycles. Conditions: 5 °C/min heating rate, air atmosphere.

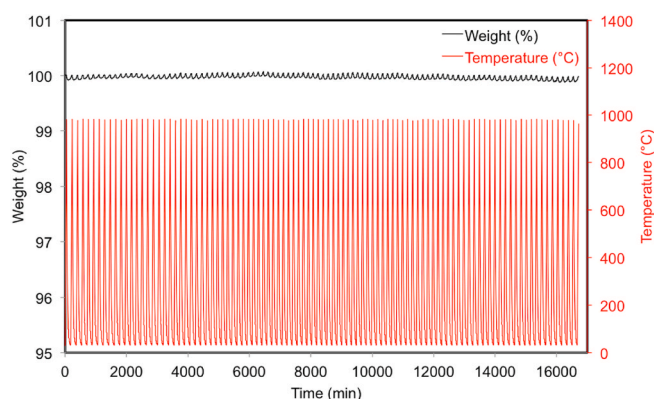


**Fig. 14.** TG analysis of Clay/4.7TCP sample with 100 consecutive heating/cooling cycles. Conditions: Heating from 25 to 1000 °C (20 °C/min heating rate) under an air flow; cooling freely from 1000 °C to 25 °C under an air flow.

initial mass weighed at the beginning of TMA analysis, the bulk density of sample can be calculated along the heating program from 30 to 1000 °C.

### 3. Results and discussions

#### 3.1. Raw materials characterization

Table 2 shows the elemental composition obtained by ICP-AES of clay and TCP. For clay, the results indicate a predominance of silica and alumina. Calcium, iron, potassium, magnesium and sodium oxides are also present at lower concentrations. Other elements such as C, H, N, O and S (mostly carbonates), as well as the possible presence of minority elements, which cannot be determined by this technique, represent 15 wt% of the clay. Concerning the TCP, due to the high purity, only calcium and phosphorus oxides were identified and quantified.

The analysis of particle size distribution of natural clay and sand, which were used to constitute the clay/sand mixture used in the present study, was previously reported [45]. Briefly, natural sand was mostly composed of large particles ( $d_{10} = ca. 8 \mu\text{m}$ ,  $d_{50} = ca. 500 \mu\text{m}$ ,  $d_{90} = ca. 2050 \mu\text{m}$ ). On the other hand, natural clay contained much smaller mineral particles ( $d_{10} = ca. 1 \mu\text{m}$ ,  $d_{50} = ca. 7 \mu\text{m}$ ,  $d_{90} = ca. 50 \mu\text{m}$ ).

Fig. 1 shows the particle size distribution of the TCP additive that was used in the study. The results indicate that TCP has a bimodal particle size distribution ranging from 0.1 to 31  $\mu\text{m}$ , with an average particle size of 4  $\mu\text{m}$ . This result is supported by the SEM results (Fig. 2), displaying small and relatively heterogeneous particles size.

Fig. 3 shows the TG and DTG (differential weight loss, %/min) curves of the raw materials under the air atmosphere. For clay, a first weight loss of 2.6 wt% from the room temperature to 200 °C is attributed to the dehydration. Then, a dehydroxylation takes place between 400 and 600 °C causing a 2 wt% weight loss. The quartz transition at ca. 573 °C was also observed (Fig. 3 b). From 650 to 850 °C, the decarbonation of calcium carbonate occurs with a 4.4 wt% weight loss [36]. For TCP, the weight losses are due to surface moisture removal (around 100 °C), dehydration of hydrogenophosphate surface groups, and partial dehydroxylation of OH<sup>-</sup> groups in the apatitic structure of TCP [46].

#### 3.2. Thermogravimetry analysis

Fig. 4 shows the thermal behavior of clay ceramics doped with different percentage of TCP under the air atmosphere. In comparison with undoped clay (Fig. 4.), the addition of TCP did not modify the thermal behavior of clay matrix in the temperature range investigated. Different weight losses can be identified corresponding to the surface moisture removal, dehydration, dehydroxylation and calcium carbonate decomposition. However, the addition of TCP led to a decrease of the total weight loss, which is explained by the fact that the total weight loss of TCP is smaller than that of clay (Fig. 3). Above 850 °C, there is not further weight loss. So, clay-TCP ceramics are thermally stable up to at least 1100 °C, which is important for TES application.

#### 3.3. Density, pore volume fraction and microstructure observations

The porosity of the fired ceramics (firing conditions: 5 °C/min heating rate, 1100 °C final temperature, under air atmosphere) was first studied. The porosity decreased from 28% for the standard fired clay ceramic (without TCP addition) to respectively 25% and 23% for the ceramics containing 2 and 4.7 wt% of TCP. It may be explained by the incorporation of small TCP particles inside the porosity of clay matrix. On the other hand, at higher TCP contents of 12 wt% and 16.7 wt%, the porosity of the corresponding ceramics slightly increased to 25%, which may be due to the dehydration of OH<sup>-</sup> groups from the apatitic structure of TCP (Fig. 3).

According to the evolution of the porosity, the study on the evolution of the bulk density of the fired ceramics shows that TCP addition up to 4.7 wt% allowed increasing the bulk density of materials (from 1970 kg/m<sup>3</sup> for the standard fired clay ceramic to respectively 2070 kg/m<sup>3</sup> and 2140 kg/m<sup>3</sup> for Clay/2 TCP and Clay/4.7TCP). On the other hand, no further bulk density increase is observed at higher TCP additions of 12 and 16.7 wt%.

The mineralogical composition of three different ceramics were determined by XRD (Fig. 5). The standard ceramic (without TCP

addition) mainly contained quartz, hematite and anorthite, as well as other minority phases of feldspath and gehlenite. These crystalline phases were also observed for the ceramics doped with TCP, in which other apatitic structures were also identified (hydroxyapatite and possibly iron-doped hydroxyapatite).

Fig. 6 illustrates the micrographs of different fired ceramics by X-ray tomography. This technique mostly evidenced the presence of macropores inside the samples. The analysis of all images of each sample shows that macropores were more frequently observed in the virgin ceramic without TCP. The size and shape of pores of this virgin sample seem to be largely heterogeneous, with the presence of pores having different shapes (e.g. likely-spheres, elongated cracks etc.) and sizes (from some  $\mu\text{m}$  to hundreds  $\mu\text{m}$ ), which are classically observed for fired clay ceramics. In fact, this porosity results from different steps of clay ceramic production. First, it is due to the presence of air in the mixture during the extrusion process. Second, elongated cracks are frequently formed during the drying step, due to the irregular contraction of extruded blocks, when water leaves clay matrix [37,43]. Finally, firing step up to  $1100\text{ }^\circ\text{C}$  causes the gas release (e.g. liberation of water vapor, carbon dioxide etc.) which can also create pores [47].

For TCP-doped ceramics (Fig. 6 b, c), macropores are also present, but their shape and size seem to be much more homogeneous in comparison to those of the undoped ceramic. This explains the increase of the bulk density by adding 4.7 wt% TCP. Fine particles of TCP ( $d_{50} = 4\ \mu\text{m}$ , Fig. 1) can penetrate to the porosity of the clay matrix, which reduces the porosity of doped ceramic. In the case of Fig. 6 c, a large grain of size above  $200\ \mu\text{m}$  (dark color) was present, which contained pores under the forms of cracks. This is possibly a quartz grain, taking into account its large size. During the firing, a thermal expansion-contraction of grain (volume variation) could take place when the quartz transition occurred at ca.  $573\text{ }^\circ\text{C}$ .

Fig. 7 presents the mapping of the elements present in the virgin clay ceramic (without TCP addition) and in Clay/16.7TCP ceramic, which were fired at  $1100\text{ }^\circ\text{C}$  under air atmosphere. For the fired virgin clay (Fig. 7 a), the main elements of clay including Al, Si, Ca, K, Mg, Fe, Na, could be found, which fits well with the elemental composition by ICP-AES (Table 1). For the fired Clay/16.7TCP ceramic, calcium and mostly phosphorus are homogeneously distributed on the analyzed surface, except the zones corresponding to large particles of clay. This confirms the penetration of fine TCP particles inside the porosity of clay matrix during the ceramic production by extrusion. The next section will present the impacts of TCP penetration on the properties of TCP-doped ceramics in view of TES application.

### 3.4. Impact of TCP addition on the thermal and mechanical properties of fired TCP-doped ceramics

This section presents the effect of the TCP addition on the thermal and mechanical properties of fired ceramics. All measurements were performed at room temperature (ca.  $25\text{ }^\circ\text{C}$ ).

Fig. 8 shows the evolution of the thermal conductivity of the fired ceramics as a function of TCP content. The addition of TCP into the clay matrix allows increasing the thermal conductivity of the virgin clay ceramic up to 8 wt% TCP content. Then, the thermal conductivity seems to be more or less stabilized. At 8 wt% TCP content, the thermal conductivity reaches the highest value of  $1.05\text{ W/m/K}$ , which is 31.2% higher than that of the virgin clay ceramic ( $0.80\text{ W/m/K}$ ). This can be explained by the microstructural modifications, such as the shape and size of the porosity, by TCP addition, as discussed in the previous section [48–50].

The evolution of the specific heat capacity of the fired ceramics as a function of TCP content is presented in Fig. 9. The TCP addition into the clay matrix has no effect on the specific heat, which is stable around  $0.74\text{ kJ/kg/K}$  (and which is also close to the value obtained for pure TCP pellet prepared with a hydraulic press), despite the microstructural modifications discussed above. Probably fine TCP particles were only

physically inserted inside the clay matrix, but there was no formation of new chemical bond between TCP and different components of the clay matrix. Further investigations are needed to evidence the chemical aspect of these mixtures between TCP and the clay.

The evolution of the mechanical strength of fired ceramics as a function of TCP content is presented in Fig. 10. Globally, the TCP addition allows increasing the mechanical strength of the fired ceramics, and the optimal value seems to be obtained at 4.7 wt% TCP content (average value of  $18\text{ MPa}$ , or 15.4% higher than that of the virgin clay). This beneficial impact can be explained by the improvement of the microstructure of the fired ceramics. Fine TCP particles penetrate in the clay matrix, leading to the decrease of porosity, which improves the mechanical strength.

In view of application as TES materials, the TCP addition has positive impacts on the thermal and mechanical properties of the fired ceramics. This not only increases the mechanical strength, but also improves the low thermal conductivity of the virgin clay. Consequently, this improves heat transfer between heat transfer fluid (HTF) these fired ceramics as monolithic storage media, and offers more flexibility in the design of TES system. Taking into account the properties of the elaborated materials, the TCP content of 4.7 wt% appears as the best value, among the investigated ceramics. At this TCP content, Clay/4.7TCP ceramic has the lowest porosity, the highest bulk density, the highest mechanical strength (Fig. 10), while keeping a good thermal conductivity (Fig. 8) and specific heat capacity (Fig. 9). Thus, Clay/4.7TCP ceramic was selected for further characterization. Virgin clay ceramic was also investigated as reference.

In order to confirm the advantage of the TCP addition on the properties of the fired ceramics, it is indispensable to investigate these materials under dynamic conditions, which is presented in the next section.

### 3.5. Thermo-physical, thermo-mechanical properties and thermal stability under dynamic conditions

Since TES materials will be submitted to repeated heating-cooling cycles, it is important to investigate the thermal behavior of those materials under dynamic conditions. Fig. 11 presents the evolution of the thermal conductivity of the virgin clay ceramic and Clay/4.7TCP ceramic during three consecutive heating from  $25$  to  $1000\text{ }^\circ\text{C}$  under the air atmosphere. Practically, for each measurement, the sample, which was already fired under the air at  $1100\text{ }^\circ\text{C}$ , was heated to  $1000\text{ }^\circ\text{C}$  ( $5\text{ }^\circ\text{C}/\text{min}$  heating rate) and the thermal diffusivity was recorded which allowed calculating the thermal conductivity of the 1st cycle, according to Eq. (3). Then, the sample is cooled down under uncontrolled cooling rate, and consequently, the thermal diffusivity was not recorded. At  $25\text{ }^\circ\text{C}$ , the sample was heated again to  $1000\text{ }^\circ\text{C}$  ( $5\text{ }^\circ\text{C}/\text{min}$  heating rate) to obtain the thermal conductivity of the 2nd cycle. This procedure was also repeated for the 3rd cycle.

In Fig. 11, both the virgin clay ceramic and Clay/4.7TCP ceramic show similar profiles of the thermal conductivity. For the virgin clay ceramic and during the 1st heating, the thermal conductivity increases from  $0.76$  at  $25\text{ }^\circ\text{C}$  to  $0.87\text{ W/m/K}$  at  $200\text{ }^\circ\text{C}$ . Then, it continuously decreases to  $0.73\text{ W/m/K}$  in the temperature range of  $200$ – $500\text{ }^\circ\text{C}$ , before growing to  $1.08\text{ W/m/K}$  in the temperature range of  $500$ – $1000\text{ }^\circ\text{C}$ . The minimal value of the thermal conductivity around  $500\text{ }^\circ\text{C}$  may be related to the quartz inversion ( $\alpha$ – $\beta$  transition) of the clay matrix, which occurs at around  $573\text{ }^\circ\text{C}$  [51]. During the 2nd and 3rd heating, the profiles of the thermal conductivity are similar to each other. However, some differences can be observed between the thermal conductivity of the 2nd and the 3rd heating and that of the 1st heating. This indicates that the microstructure of the fired virgin clay ceramic was not completely stabilized after the firing step. Physico-chemical phenomena, such as the dehydroxylation, might be not finished after the firing at  $1100\text{ }^\circ\text{C}$ , and continue during the 1st, even the 2nd or 3rd heating, and cause the differences in the thermal conductivity during the heating cycles.

For Clay/4.7TCP ceramic, as expected, the TCP addition allows increasing the thermal conductivity up to 44% in the temperature range investigated (25–1000 °C), in comparison with the virgin clay ceramic. During the three consecutive heating cycles, Clay/4.7TCP ceramic shows the similar behavior to that observed for the virgin clay ceramic. During the 1st heating, the thermal conductivity increases from 1.10 W/m/K at 25 °C to 1.14 W/m/K at 200 °C. Then, it decreases to 0.96 W/m/K at 500 °C before increasing to 1.16 W/m/K at 1000 °C. The thermal conductivity recorded for the 2nd and the 3rd heating is relatively repeated, indicating that the microstructure of this ceramic is mostly stable after the firing and the 1st heating.

Fig. 12 (a) and (b) present the evolution of the specific heat capacity and the bulk density of the fired virgin clay ceramic and Clay/4.7TCP ceramic as functions of the temperature. Note that bulk density in Fig. 12 (b) was calculated from TMA and TG analyses, as explained in the experimental section. Both ceramics have the comparable specific heat capacity in the temperature range of 25–1000 °C. Increasing the temperature leads to a considerable increase of the specific heat capacity, which reaches 1.19 kJ/kg/K at 1000 °C for Clay/4.7TCP, or 55% higher than the value at 25 °C (0.77 kJ/kg/K). However, increasing the temperature Clay/4.7TCP also leads to a small decrease of its bulk density from 2140 kg/m<sup>3</sup> at 1000 °C to 2100 kg/m<sup>3</sup> at 25 °C, or a decrease of 2%. Consequently, the specific energy density of Clay/4.7TCP, calculated as the product of the specific heat capacity and the bulk density, continuously increases from 1647.8 kJ/m<sup>3</sup>/K at 25 °C to 2499 kJ/m<sup>3</sup>/K at 1000 °C (Fig. 12 (c)). This is very important for TES materials since the increase of the specific energy density allows decreasing the global cost of the heat storage. It is worth noticing that the specific energy density of the Clay/4.7TCP ceramic is much higher than that of other materials reported in the literature, such as concrete (2272 kJ/m<sup>3</sup>/K at 350 °C [30]), natural rocks (2180 kJ/m<sup>3</sup>/K at 400 °C [26]), ceramic from industrial inorganic wastes (2496–3226 kJ/m<sup>3</sup>/K at 25–1000 °C [52,53]), or molten salts (2643 kJ/m<sup>3</sup>/K at 600 °C [54]). Furthermore, an average thermal expansion coefficient (TEC) of 6.10<sup>-6</sup>/°C (Supplementary information SI. 1) was also recorded for Clay/4.7TCP, which is ca. 48% lower than the values of concrete and ceramic from industrial inorganic wastes [30,52].

Fig. 13 shows the evolution of the Young's modulus during three consecutive heating/cooling cycles of the fired virgin clay ceramic and Clay/4.7TCP ceramic. For each ceramic, the sample, which was already fired at 1000 °C, was heated from room temperature to 1050 °C (5 °C/min heating rate), then cooled down to room temperature (5 °C/min cooling rate). During this first heating/cooling cycle, the sample was mechanically excited according to the norm ASTM E1876 [44], and the resonance frequency was recorded which allowed calculating the Young's modulus. This procedure was repeated for the 2nd and the 3rd heating/cooling cycles. The results in Fig. 13 reveal the similar behavior of the two ceramics, and highlight the positive impact of the TCP addition on the mechanical resistance. At room temperature, the Young's modulus is equal to 22.6 GPa for the virgin clay ceramic, and 28.3 GPa for Clay/4.7TCP ceramic. So, an increase of 25% of the mechanical resistance was obtained by the TCP addition (4.7 wt%), in accordance with the results obtained by flexural measurement (Fig. 10). From room temperature to 550 °C, the Young's modulus slightly growth from 22.6 to 25 GPa and from 28.3 to 32.5 GPa for the virgin clay ceramic and Clay/4.7TCP ceramic, respectively. A strong evolution is observed around 550–650 °C, which must be due to the quartz inversion of the clay matrix, which takes place at around 573 °C [51]. Then, the Young's modulus is more or less stable up to 1050 °C for both materials. For each cycle of heating/cooling, a hysteresis could be observed, which is principally due to the opening and closing of microstructural de-cohesion of materials [55,56]. This means that up to 1050 °C, the temperature has no negative effect on the mechanical resistance of both materials, which is important for their utilization in TES.

TES materials should be thermally stable during repeated heating/cooling cycles. To validate this criterion, Clay/4.7TCP was analyzed by

100 consecutive heating/cooling cycles using TG analysis under the air flow. The sample was heated from 25 to 1000 °C (20 °C/min heating rate), then freely cooled down to 25 °C, and this procedure was repeated 100 times. Fig. 14 shows the temperature profiles and the evolution of TG signal of the sample during these 100 cycles, where its thermal behavior is identically repeated. For each cycle, a “weight loss” of ca. 0.2% was recorded during the heating to 1000 °C. In fact, this mass variation must be due to the measurement under hot air (1000 °C), and the sample could recover its initial mass during the cooling to 25 °C. After 100 cycles, there was neither mass variation, nor color change. In the other words, the sample was completely conserved.

#### 4. Conclusions

This work investigated the impact of phosphate (TCP) addition on the microstructure and properties of fired clay ceramics in view of the design of new performing TES materials. Salient conclusions arising from this work are summarized below.

- The addition of TCP to the clay matrix allows improving most of the properties of fired clay ceramic: decrease of porosity, and increase of thermal conductivity, bulk density, and mechanical resistance. Among the TCP content investigated, the addition of 4.7w.% seems to be the best choice.
- The characterization of the best material (Clay/4.7TCP) under the dynamic conditions shows that the material is thermally stable and its specific energy density continuously increases during the heating from 25 to 1000 °C.

Clay/4.7TCP sample possesses promising properties for a TES material in the temperature range of 25–1000 °C: bulk density = 2140–2120 kg/m<sup>3</sup>; thermal conductivity = 1–1.16 W/m/K; specific heat capacity = 0.7–1.2 kJ/kg/K; specific energy density = 1647.8–2499 kJ/m<sup>3</sup>/K; Young's modulus = 28–45 GPa; TEC = 6.10<sup>-6</sup>/°C; and a perfect thermal stability during 100 cycles of repeated heating/cooling. Thus, this material seems to be suitable for application in TES. Future work would be focused on the identification of other phosphates, clay deposits, and other ceramic production techniques, such as pressing, in order to optimize the bulk density of material. The validation at the pilot scale is also indispensable before a possible industrial deployment.

#### Funding

This study was funded by Prayon and OCP.

#### Declaration of competing interest

The authors declare that they have no known competing financial interests or personal relationships that could have appeared to influence the work reported in this paper.

#### Acknowledgment

The authors gratefully thank Prayon and OCP for the financial supports. The technical help from our colleagues at the RAPSODEE research center is also acknowledged.

#### Appendix A. Supplementary data

Supplementary data to this article can be found online at <https://doi.org/10.1016/j.oceram.2023.100346>.

#### References

- [1] IEA, Statistics Report: Renewables Information - Overview, 2020.
- [2] BP, BP Statistical Review of World Energy, 2018.

- [3] IEA, *Renewables 2017: Analysis and Forecasts to 2022*, 2017.
- [4] IRENA, *Renewable Power Generation Costs in 2017*, 2017.
- [5] P. Pardo, A. Deydier, Z. Anxionnaz-Minvielle, S. Rouge, M. Cabassud, P. Cognet, A review on high temperature thermochemical heat energy storage, *Renew. Sustain. Energy Rev.* 32 (2014) 591–610, <https://doi.org/10.1016/j.rser.2013.12.014>.
- [6] U. Pelay, L. Luo, Y. Fan, D. Stitou, M. Rood, Thermal energy storage systems for concentrated solar power plants, *Renew. Sustain. Energy Rev.* 79 (2017) 82–100, <https://doi.org/10.1016/j.rser.2017.03.139>.
- [7] A. Gil, M. Medrano, I. Martorell, A. Lazaro, P. Dolado, B. Zalba B, L.F. Cabeza, State of the art on high temperature thermal energy storage for power generation. Part 1-Concepts, materials and modelling, *Renew. Sustain. Energy Rev.* 14 (1) (2010) 31–55, <https://doi.org/10.1016/j.rser.2009.07.035>.
- [8] S. Kuravi, J. Trahan, D.Y. Goswami, M.M. Rahman, E.K. Stefanakos, Thermal energy storage technologies and systems for concentrating solar power plants, *Prog. Energy Combust. Sci.* 39 (4) (2013) 285–319, <https://doi.org/10.1016/j.pecs.2013.02.001>.
- [9] M. Medrano, A. Gil, I. Martorell, X. Potau, L.F. Cabeza, State of the art on high-temperature thermal energy storage for power generation. Part 2-Case studies, *Renew. Sustain. Energy Rev.* 14 (1) (2010) 56–72, <https://doi.org/10.1016/j.rser.2009.07.036>.
- [10] J. Xu, R.Z. Wang, Y. Li, A review of available technologies for seasonal thermal energy storage, *Sol. Energy* 103 (2014) 610–638, <https://doi.org/10.1016/j.solener.2013.06.006>.
- [11] Y. Hou, R. Vidu, P. Stroevé, Solar energy storage methods, *Ind. Eng. Chem. Res.* 50 (15) (2011) 8954–8964, <https://doi.org/10.1021/ie2003413>.
- [12] L.F. Cabeza, I. Martorell, L. Miro, A.I. Fernandez, C. Barreneche, *Introduction to thermal energy storage (TES) systems*, in: L.F. Cabeza (Ed.), *Advances in Thermal Energy Storage Systems*, Elsevier, 2015, pp. 1–28.
- [13] G. Alva, L. Liu, X. Huang, G. Fang, Thermal energy storage materials and systems for solar energy applications, *Renew. Sustain. Energy Rev.* 68 (2017) 693–706, <https://doi.org/10.1016/j.rser.2016.10.021>.
- [14] K. Vignaroban, X. Xu, A. Arvay, K. Hsu, A.M. Kannan, Heat transfer fluids for concentrating solar power systems – a review, *Appl. Energy* 146 (2015) 383–396, <https://doi.org/10.1016/j.apenergy.2015.01.125>.
- [15] Andasol 1 CSP project. <https://solarpaces.nrel.gov/project/andasol-1>.
- [16] S.E. Trabelsi, R. Chargui, L. Qoaider, A. Liqueina, A. Guizani, Techno-economic performance of concentrating solar power plants under the climatic conditions of the southern region of Tunisia, *Energy Convers. Manag.* 119 (2016) F203–F214, <https://doi.org/10.1016/j.enconman.2016.04.033>.
- [17] F. Dinter, D.M. Gonzalez, Reliability and economic benefits of CSP with thermal energy storage: first year of operation of ANDASOL 3, *Energy Proc.* 49 (2014) 2472–2481, <https://doi.org/10.1016/j.egypro.2014.03.262>.
- [18] I. Noor midelt, Le Maroc construit une centrale solaire hybride hors norme. <https://www.masen.ma/fr/actualites-masen/noor-midelt-i-le-maroc-construit-une-centrale-solaire-hybride-hors-norme>.
- [19] IEA, *Technology Roadmap Solar Thermal Electricity - 2014*, edition, 2014.
- [20] S. Ushak, A.G. Fernandez, M. Grageda, Using molten salts and other liquid sensible storage media in thermal energy storage (TES) systems, in: L.F. Cabeza (Ed.), *Advances in Thermal Energy Storage Systems*, Woodhead Publishing, 2015, pp. 49–63.
- [21] D. Barlev, R. Vidu, P. Stroevé, Innovation in concentrated solar power, *Sol. Energy Mater. Sol. Cell.* 95 (10) (2011) 2703–2725, <https://doi.org/10.1016/j.solmat.2011.05.020>.
- [22] M.E. Navarro, M. Martinez, A. Gil, A.I. Fernandez, L.F. Cabeza, R. Olives, X. Py, Selection and characterization of recycled materials for sensible thermal energy storage, *Sol. Energy Mater. Sol. Cell.* 107 (2012) 131–135, <https://doi.org/10.1016/j.solmat.2012.07.032>.
- [23] S. Khare, M. Dell'Amico, C. Knight, S. McGarry, Selection of materials for high temperature sensible energy storage, *Sol. Energy Mater. Sol. Cell.* 115 (2013) 114–122, <https://doi.org/10.1016/j.solmat.2013.03.009>.
- [24] K.G. Allen, T.W. von Backström, D.G. Kroger, A.F.M. Kisters, Rock bed storage for solar thermal power plants: rock characteristics, suitability, and availability, *Sol. Energy Mater. Sol. Cell.* 126 (2014) 170–183, <https://doi.org/10.1016/j.solmat.2014.03.030>.
- [25] R. Tiskatine, R. Oaddia, R. Ait El Cadi, A. Bazgaoui, L. Bourirden, A. Aharoune, A. Ihlal, Suitability and characteristics of rocks for sensible heat storage in CSP plants, *Sol. Energy Mater. Sol. Cell.* 169 (2017) 245–257, <https://doi.org/10.1016/j.solmat.2017.05.033>.
- [26] Y. Jemmal, N. Zari, M. Maaroufi, Experimental characterization of siliceous rocks to be used as filler materials for air-rock packed beds thermal energy storage systems in concentrated solar power plants, *Sol. Energy Mater. Sol. Cell.* 171 (2017) 33–42, <https://doi.org/10.1016/j.solmat.2017.06.026>.
- [27] D.W. Waples, J.S. Waples, A review and evaluation of specific heat Capacities of rocks, minerals, and subsurface fluids. Part 1: minerals and nonporous rocks, *Nat. Resour. Res.* 13 (2) (2004) 97–122, <https://doi.org/10.1023/B:NARR.0000032647.41046.e7>.
- [28] I. Iosif Stylianou, S. Tassou, P. Christodoulides, I. Panayides, G. Florides, Measurement and analysis of thermal properties of rocks for the compilation of geothermal maps of Cyprus, *Renew. Energy* 88 (2016) 418–429, <https://doi.org/10.1016/j.renene.2015.10.058>.
- [29] D. Laing, D. Lehmann, M. Fiß, C. Bahl, Test results of concrete thermal energy storage for parabolic trough power plants, *J. Sol. Energy Eng.* 131 (4) (2009), 041007, <https://doi.org/10.1115/1.1319784>.
- [30] D. Laing, S. Sunft, Using concrete and other solid storage media in thermal energy storage (TES) systems, in: L.F. Cabeza (Ed.), *Advances in Thermal Energy Storage Systems*, Woodhead Publishing, 2015, pp. 65–86, <https://doi.org/10.1533/9781782420965.1.65>.
- [31] M. Martins, U. Villalobos, T. Delclos, P. Armstrong, P.G. Bergan, N. Calvet, New concentrating solar power facility for testing high temperature concrete thermal energy storage, *Energy Proc.* 75 (2015) 2144–2149, <https://doi.org/10.1016/j.egypro.2015.07.350>.
- [32] E. John, M. Hale, P. Selvam, Concrete as a thermal energy storage medium for thermochemical solar energy storage systems, *Sol. Energy* 96 (2013) 194–204, <https://doi.org/10.1016/j.solener.2013.06.033>.
- [33] A. Gutierrez, L. Miro, A. Gil, J. Rodriguez-Aseguinolaza, C. Barreneche, N. Calvet, X. Py, A.I. Fernandez, M. Grageda, S. Ushak, L.F. Cabeza, Advances in the valorization of waste and by-product materials as thermal energy storage (TES) materials, *Renew. Sustain. Energy Rev.* 59 (2016) 763–783, <https://doi.org/10.1016/j.rser.2015.12.071>.
- [34] X. Py, N. Calvet, R. Olives, A. Meffre, P. Echegut, C. Bessada, E. Veron, S. Ory, Recycled material for sensible heat based thermal energy storage to be used in concentrated solar thermal power plant, *J. Sol. Energy Eng.* 133(3):1–7. <https://doi.org/10.1016/j.egypro.2014.03.111>.
- [35] A. Kere, X. Py, R. Olives, V. Goetz, N. Sadiki, E. Mercier, High temperature thermal energy storage material from vitrified coal-fired power plant Fly-Ash, *12<sup>th</sup> Int Conf Energy Storage* (2012) 1–10.
- [36] P.M. Nigay, T. Cutard, A. Nzihou, The impact of heat treatment on the microstructure of a clay ceramic and its thermal and mechanical properties, *Ceram. Int.* 43 (2) (2017) 1747–1754, <https://doi.org/10.1016/j.ceramint.2016.10.084>.
- [37] P.M. Nigay, A. Nzihou, C.E. White, W.O. Soboyejo, Structure and properties of clay ceramics for thermal energy storage, *J. Am. Ceram. Soc.* 100 (10) (2017) 4748–4759, <https://doi.org/10.1111/jace.15014>.
- [38] W.M. Carty, U. Senapati, Porcelain-raw materials, processing, phase evolution, and mechanical behavior, *J. Am. Ceram. Soc.* 81 (2005) 3–20, <https://doi.org/10.1111/j.1151-2916.1998.tb02290.x>.
- [39] B. Régo De Vasconcelos, L. Zhao, P. Sharrock, A. Nzihou, D. Pham Minh, Catalytic transformation of carbon dioxide and methane into syngas over ruthenium and platinum supported hydroxyapatites, *Appl. Surf. Sci.* 390 (2016) 141–156, <https://doi.org/10.1016/j.apsusc.2016.08.077>.
- [40] T.S. Phan, A.R. Sane, B. Régo de Vasconcelos, A. Nzihou, P. Sharrock, D. Grouset, D. Pham Minh, Hydroxyapatite supported bimetallic cobalt and nickel catalysts for syngas production from dry reforming of methane, *Appl. Catal. B Environ.* 224 (2018) 310–321, <https://doi.org/10.1016/j.apcatb.2017.10.063>.
- [41] AFNOR, Essais pour déterminer les propriétés physiques des roches, partie 3 : détermination de la porosité, NF P94-410-3. <https://www.boutique.afnor.org/nor/me/nf-p94-410-3/roches-essais-pour-determiner-les-proprietes-physiques-des-roches-partie-3-determination-de-la-porosite/article/724514/fa106661>.
- [42] S. Min, J. Blumm, A. Lindemann, A new laser flash system for measurement of the thermophysical properties, *Thermochim. Acta* 455 (1–2) (2007) 46–49, <https://doi.org/10.1016/j.tca.2006.11.026>.
- [43] L.V. Korah, P.M. Nigay, T. Cutard, A. Nzihou, S. Thomas, The impact of the particle shape of organic additives on the anisotropy of a clay ceramic and its thermal and mechanical properties, *Construct. Build. Mater.* 125 (2016) 654–660, <https://doi.org/10.1016/j.conbuildmat.2016.08.094>.
- [44] ASTM, Standard test method for dynamic Young's modulus, shear modulus, and Poisson's ratio by impulse excitation of vibration, ASTM E1876 - 15, <https://www.astm.org/Standards/E1876.htm>. (Accessed 2 September 2022).
- [45] Pierre-Marie Nigay, Etude des transformations microstructurales de mélanges argile/biomasse lors de la cuisson et relations avec les propriétés mécaniques et thermiques, PhD thesis, IMT Mines Albi, 2015. <https://www.theses.fr/2015EMAC0001>.
- [46] D. Pham Minh, N. Lyczko, H. Sebei, A. Nzihou, P. Sharrock, Synthesis of calcium hydroxyapatite from calcium carbonate and different orthophosphate sources: a comparative study, *Mater. Sci. Eng., B* 177 (2012) 1080–1089, <https://doi.org/10.1016/j.mseb.2012.05.007>.
- [47] A.S. Sane, P.M. Nigay, D. Pham Minh, C. Toussaint, A. Germeau, N. Semlal, R. Boulif, A. Nzihou, an investigation of the physical, thermal and mechanical properties of fired-clay/SiC ceramics for thermal energy storage, *J. Therm. Anal. Calorim.* 140 (5) (2020) 2087–2096, <https://doi.org/10.1007/s10973-019-08964-5>.
- [48] G. Pia, L. Casnedi, U. Sanna, Porosity and pore size distribution influence on thermal conductivity of yttria-stabilized zirconia: experimental findings and model predictions, *Ceram. Int.* 42 (5) (2016) 5802–5809, <https://doi.org/10.1016/j.ceramint.2015.12.122>.
- [49] X. Huai, W. Wang, Z. Li, Analysis of the effective thermal conductivity of fractal porous media, *Appl. Therm. Eng.* 27 (17–18) (2007) 2815–2821, <https://doi.org/10.1016/j.applthermaleng.2007.01.031>.
- [50] D.S. Smith, A. Alzina, J. Bourret, F. Pennec, N. Tessier-Doyen, K. Otsu, H. Matsubara, P. Elser, U.T. Gonzenbach, Thermal conductivity of porous materials, *J. Mater. Res.* 28 (17) (2013) 2260–2272, <https://doi.org/10.1557/jmr.2013.179>.
- [51] J. Bourret, N. Tessier-Doyen, R. Guinebretiere, E. Joussein, D.S. Smith, Anisotropy of thermal conductivity and elastic properties of extruded clay-based materials: evolution with thermal treatment, *Appl. Clay Sci.* (2015) 116–117, <https://doi.org/10.1016/j.clay.2015.08.006>, 150–157.
- [52] A. Meffre, *Matériaux de stockage thermique haute température issus de la valorisation de matières premières secondaires inorganiques*, PhD thesis, Université de Perpignan Via Domitia, 2012. <http://theses.fr/2013PERP1238>.
- [53] A. Kere, *Stockage d'électricité par compression adiabatique d'air*, PhD thesis, Université de Perpignan Via Domitia, 2014. <http://theses.fr/2014PERP1248>.

- [54] R. Serrano-Lopez, J. Fradera, S. Cuesta-Lopez, Molten salts database for thermal energy applications, *Chem. Eng. Process: Process Intensif.* 73 (2013) 87–102, <https://doi.org/10.1016/j.cep.2013.07.008>.
- [55] N. Tessier-Doyen, X. Grenier, M. Huger, D.S. Smith, D. Fournier, J.P. Roger, Thermal conductivity of alumina inclusion/glass matrix composite materials: local and macroscopic scales, *J. Eur. Ceram. Soc.* 27 (2007) 2635–2640, <https://doi.org/10.1016/j.jeurceramsoc.2006.09.017>.
- [56] M. Huger, *Elasticité à haute température de matériaux céramiques : effet des hétérogénéités*. Habilitation à diriger des recherches (HDR), Université de Limoges, 2008.